

Exchange coupling constants at finite temperature

S. Mankovsky,¹ S. Polesya,¹ and H. Ebert¹

¹*Department Chemie, Physikalische Chemie, Universität München, Butenandstr. 5-13, 81377 München, Germany*
(Dated: June 23, 2020)

An approach to account for the effect of thermal lattice vibrations when calculating exchange coupling parameters is presented on the basis of the KKR (Korringa-Kohn-Rostoker) Green function method making use of the alloy analogy model. Using several representative systems, it is shown that depending on the material the effect of thermal lattice vibrations can have a significant impact on the isotropic exchange as well as anisotropic Dzyaloshinskii-Moriya interactions (DMI). This should lead in turn to an additional contribution to the temperature dependence of the magnetic properties of solids, which cannot be neglected in the general case. As an example, we discuss such an influence on the critical temperature of various magnetic phase transitions. In particular, in the case of skyrmion hosting materials, a strong impact of lattice vibrations on the DMI is an additional source for temperature dependent skyrmion stability which should be taken into consideration.

PACS numbers: 71.15.-m, 71.55.Ak, 75.30.Ds

A. INTRODUCTION

The impact of finite temperatures on the various physical material properties is one of the most important issues in solid state physics that is discussed in the literature with respect to various aspects. This holds in particular for finite temperature magnetic and transport properties of materials calculated on an ab-initio level. For that purpose, a very efficient approach – the so-called alloy analogy model – has been introduced recently¹, that allows to account for the impact of temperature induced lattice vibrations and spin fluctuations on linear response properties, as for example the electrical and spin conductivity, the Gilbert damping and others. In these cases, the corresponding response tensor χ_{AB} may be written as $\chi_{AB} \propto \text{Tr} \langle A \Im G^+ B \Im G^+ \rangle_T$, where the operators A and B represent the relevant observable and perturbation, respectively, while G^+ stands for the retarded Green function². Within the alloy analogy model lattice vibrations and spin fluctuations are treated as uncorrelated, quasi-static atomic displacements and spin tiltings, respectively, with an amplitude depending on temperature. Following the scheme used to calculate the residual resistivity of disordered alloys^{2,3} by means of the single-site Coherent Potential Approximation (CPA), the thermal average $\langle \dots \rangle_T$ of a linear response quantity is obtained as the configurational average over a set of appropriately chosen set of atomic displacements and spin tiltings using the CPA alloy theory^{1,4,5}.

The central idea of the alloy analogy model was used already previously to account for thermal magnetic disorder when dealing with finite-temperature magnetic properties by means of first-principles calculations done on the basis of the disordered local moment (DLM) model⁶⁻⁸. This approach was formulated at the beginning on a non-relativistic level. Its extension to the relativistic disorder local moment (RDLM) model allowed in particular to investigate the impact of thermal spin disorder on the magneto-crystalline anisotropy (MCA)^{9,10}.

So far, most calculations of the exchange parameters

have been performed for ideal crystal structures assuming the *lattice temperature* $T_{\text{lat}} = 0$ K. Even for this situation, already a pronounced dependency of the results on the specific atomic positions could be observed for some cases^{11,12}. The significant influence of lattice vibrations on the magnon excitations of fcc Fe has been reported for example by Sabiryayov and Jaswal¹³, who calculated the exchange coupling parameters accounting for corrections due to atomic displacements using a frozen-phonon scheme. A substantial change for the exchange coupling parameters in bcc Fe was also reported to be induced by a Burgers type lattice distortion which can be connected to the single N point TA_1 phonon mode¹⁴. Recently, a strong impact of lattice vibrations on the electronic structure and magnetic properties of materials was shown employing the disordered local moments molecular dynamics (DLM-MD) method^{15,16}. This approach was also used to investigate corresponding temperature induced changes of the exchange coupling parameters, associated with thermal lattice vibrations¹⁷. Note that these DLM-MD calculations make use of supercell technique to simulate thermal atomic displacements in the system. Di Gennaro et al.¹⁸ have investigated the combined effects of 'phononic' and 'magnonic' temperatures on the spin-wave dispersion, stiffness, and Curie temperatures of Fe, Ni, and permalloy by combining first-principles methods with model Hamiltonians. Following the idea reported in Ref. 13, the authors take into account corresponding corrections to the exchange parameters, associated with the thermal root-mean-square atomic displacements at a given temperature.

Below we present a scheme to account within the framework of the alloy analogy model for thermal lattice vibrations when calculating exchange coupling parameters. As will be demonstrated by various examples, such calculations can be done on the basis of a ferromagnetic state or a more realistic paramagnetic DLM reference state.

I. THEORETICAL BACKGROUND

In the following the temperature dependence of the parameters of the extended Heisenberg Hamiltonian

$$H_{ex} = - \sum_{ij} J_{ij} (\hat{e}_i \cdot \hat{e}_j) - \sum_{ij} \vec{D}_{ij} [\hat{e}_i \times \hat{e}_j]. \quad (1)$$

will be considered. Here J_{ij} is the isotropic exchange coupling parameter connected with the spin moments on sites i and j pointing along the directions \hat{e}_i and \hat{e}_j , respectively, while \vec{D}_{ij} represents the Dzyaloshinskii-Moriya (DM) interaction. We will focus first of all on the properties of the isotropic exchange parameters J_{ij} , which are given by the average over the diagonal elements of the exchange coupling tensor¹⁹. Making use of relativistic multiple-scattering formalism the elements of this tensor can be written for $T = 0$ K as²⁰

$$J_{ij}^{\alpha_i \alpha_j} = -\frac{1}{2\pi} \Im \int dE \text{Trace} \Delta \underline{V}^{\alpha_i} \underline{\mathcal{T}}^{ij} \Delta \underline{V}^{\alpha_j} \underline{\mathcal{T}}^{ji}. \quad (2)$$

Here $\underline{\mathcal{T}}^{ij}$ is the so-called scattering path operator connecting sites i and j with the underline indicating matrices in the $\Lambda = (\kappa, \mu)$ -representation²¹. The corresponding on-site coupling for site i is represented by the matrix

$$\Delta V_{\Lambda\Lambda'}^{i\alpha} = \int d^3r Z_{\Lambda}^{\times}(\vec{r}) \beta \sigma_{\alpha} B(r) Z_{\Lambda'}(\vec{r}), \quad (3)$$

where α is one of the standard Dirac matrices, σ_{α} is a 4×4 -Pauli matrix²¹ and $B(r)$ is the spin-dependent part of the exchange-correlation potential set up within local spin-density theory²⁰. Finally, the wave functions $Z_{\Lambda}(\vec{r})$ are solutions to the Dirac equation normalized according to the relativistic multiple-scattering formalism²².

To apply the expression in Eq. (2) for the case of lattice vibrations at finite temperatures, we use again the alloy analogy model based on the adiabatic approximation. This implies that a discrete set of N_v displacement vectors $\Delta \vec{R}_v^q(T)$ with probability x_v^q ($v = 1, \dots, N_v$) is constructed for each basis atom q within the crystallographic unit cell. The vectors $\Delta \vec{R}_v^q(T)$ are connected with the temperature dependent root mean square displacement $(\langle u^2 \rangle_T)^{1/2}$ according to the relation:

$$\sum_{v=1}^{N_v} x_v^q |\Delta \vec{R}_v^q(T)|^2 = \langle u_q^2 \rangle_T. \quad (4)$$

For the applications presented below, the temperature dependent root mean square displacement is estimated using Debye's theory, providing a simple connection between $\langle u_q^2 \rangle_T$ and the *lattice temperature*.

Each displacement vector $\Delta \vec{R}_v(T)$ determines a corresponding U-matrix \underline{U}_v that describes for all matrices in the Λ -representation the coordinate transformation from a shifted atom position to the original equilibrium position. This allows in particular to connect the single-site t-matrix \underline{t}_v for a shifted atom to the common global frame

of reference used by the multiple scattering calculations. Within the alloy analogy model, each member in the set of N_v displacement vectors $\Delta \vec{R}_v(T)$ can now be seen as a pseudo-component of a multi-component pseudo alloy. As for a substitutional alloy, the site diagonal configurational average can this way be determined by solving the multi-component CPA equations referring to the global frame of reference:

$$\underline{\mathcal{T}}_{\text{CPA}} = \sum_{v=1}^{N_v} x_v \underline{\mathcal{T}}_v \quad (5)$$

$$\underline{\mathcal{T}}_v = [(\underline{t}_v)^{-1} - (\underline{t}_{\text{CPA}})^{-1} + (\underline{\mathcal{T}}_{\text{CPA}})^{-1}]^{-1} \quad (6)$$

$$\underline{\mathcal{T}}_{\text{CPA}} = \frac{1}{\Omega_{\text{BZ}}} \int_{\Omega_{\text{BZ}}} d^3k [(\underline{t}_{\text{CPA}})^{-1} - \underline{G}(\vec{k}, E)]^{-1}, \quad (7)$$

where the CPA medium is described by a corresponding CPA single-site t-matrix $\underline{t}_{\text{CPA}}$ and scattering path operator $\underline{\mathcal{T}}_{\text{CPA}}$. The first of these equations expresses the requirement for the mean-field CPA medium that embedding of a component v into the medium should not lead in the average to an additional scattering, with Eq. (6) giving the corresponding scattering path operator $\underline{\mathcal{T}}_v$ for the embedded component v . Finally, Eq. (7) gives $\underline{\mathcal{T}}_{\text{CPA}}$ by a Brillouin zone integral in terms of $\underline{t}_{\text{CPA}}$ and the so-called KKR structure constants $\underline{G}(\vec{k}, E)$ ²³.

Assuming – in line with the adiabatic approximation – a frozen potential for the displaced atoms and neglecting correlations between the atomic displacements, Eqs. (5) to (7) allow to evaluate of the necessary thermal configurational averaging when dealing with Eq. (2) for finite temperatures. This way one gets for the temperature dependent exchange coupling constants:

$$\bar{J}_{ij}^{\alpha_i \alpha_j} = -\frac{1}{2\pi} \Im \int dE \text{Trace} \langle \Delta \underline{V}^{\alpha_i} \underline{\mathcal{T}}^{ij} \Delta \underline{V}^{\alpha_j} \underline{\mathcal{T}}^{ji} \rangle_c, \quad (8)$$

where $\langle \dots \rangle_c$ represents the configurational average with respect to the set of displacements. In all calculations we have used a set of $N_v = 14$ displacements as increasing N_v led only to minor changes to the final results. As discussed for example in the context of the electrical conductivity, dealing with a configurational average as occurring in Eq. (8) leads to the so-called vertex corrections^{2,3}. As the expression in Eq. (8) refers explicitly to a specific pair of sites, these have been ignored here; i.e. the configuration average has been simplified to $\langle \Delta \underline{V}^{\alpha} \underline{\mathcal{T}}^{ij} \rangle_c \langle \Delta \underline{V}^{\beta} \underline{\mathcal{T}}^{ji} \rangle_c$.

II. COMPUTATIONAL DETAILS

The results presented below are based on self-consistent first-principles electronic structure calculations performed using the spin-polarized relativistic Korringa Kohn Rostoker Green function (SPR-KKR-GF) method^{23,24}, using the atomic sphere approximation (ASA). The local spin density approximation (LSDA) to spin density functional theory (SDFT) has been used

with a parametrization for the exchange and correlation potential as given by Vosko *et al.*²⁵. For the angular momentum expansion of the Green function the angular momentum cutoff $l_{\max} = 3$ was used. Within the present work, the following systems have been considered: bcc Fe ($a = 5.40$ a.u.), fcc Ni ($a = 6.65$ a.u.), ferromagnetic ($a = 5.66$ a.u.) and anti-ferromagnetic ($a = 5.63$ a.u.) B2 FeRh, 1ML Fe on the (111) surface of Pt ($a = 7.40$ a.u. for fcc Pt), and 1ML Fe on the (111) surface of Au ($a = 7.68$ a.u. for fcc Au) with the corresponding structure parameters given in atomic units, i.e. as multiples of the Bohr radius, in parentheses. The calculations for 1ML Fe/Pt(111) and 1ML Fe/Au(111) have been performed using a supercell geometry with a (1ML Fe/3ML Pt(Au)/5ML ES) supercell (where ES stands for empty sphere), with Fe occupying ideal fcc positions, i.e. without optimization of the interlayer distance. A k-mesh with $25 \times 25 \times 25$ grid points was used for the integration over the BZ of the three-dimensional bulk systems and with $46 \times 46 \times 5$ grid points for 1ML Fe on the (111) surface of Pt or Au, respectively. For the calculations of the exchange parameters as a function of the occupation the corresponding energy integration has been performed using an energy mesh with 200 energies having a constant imaginary part of 1 meV.

III. RESULTS

As it is mentioned above, one may expect that the modification of the electronic structure due to thermal lattice vibrations will not only influence transport and other response properties, but also the exchange coupling parameters. That this is indeed the case is demonstrated in the following for the elemental ferromagnets bcc Fe and fcc Ni, B2 bulk FeRh, as well as for a Fe monolayer on Pt(111) as representative examples.

The isotropic exchange coupling parameters J_{ij} calculated for the FM reference state of bcc Fe are plotted in Fig. 1 (a) for different amplitudes of thermal lattice vibrations related to a corresponding *lattice temperature* T_{lat} according to the Debye model. As one can see, there are indeed pronounced modifications of the exchange coupling parameters due to the lattice vibrations that depend strongly on the considered pair of sites. By far the most significant changes are found for the nearest-neighbor interaction parameters that decrease strongly with an increase of the amplitude of the thermal displacements or the *lattice temperature*, respectively. This in turn should have a corresponding impact on the Curie temperature T_C . Within the mean-field approximation (MFA), T_C is essentially given by a sum $\sum_j J_{ij}$ over the coupling parameters allowing therefore in a simple way to monitor the dependency of T_C on the effective *lattice temperature* T_{lat} or, equivalently, on the temperature dependent rms displacement $(\langle u^2 \rangle_T)^{1/2}$. Fig. 2 (circles) shows corresponding results for T_C as a function of $(\langle u^2 \rangle_T)^{1/2}$

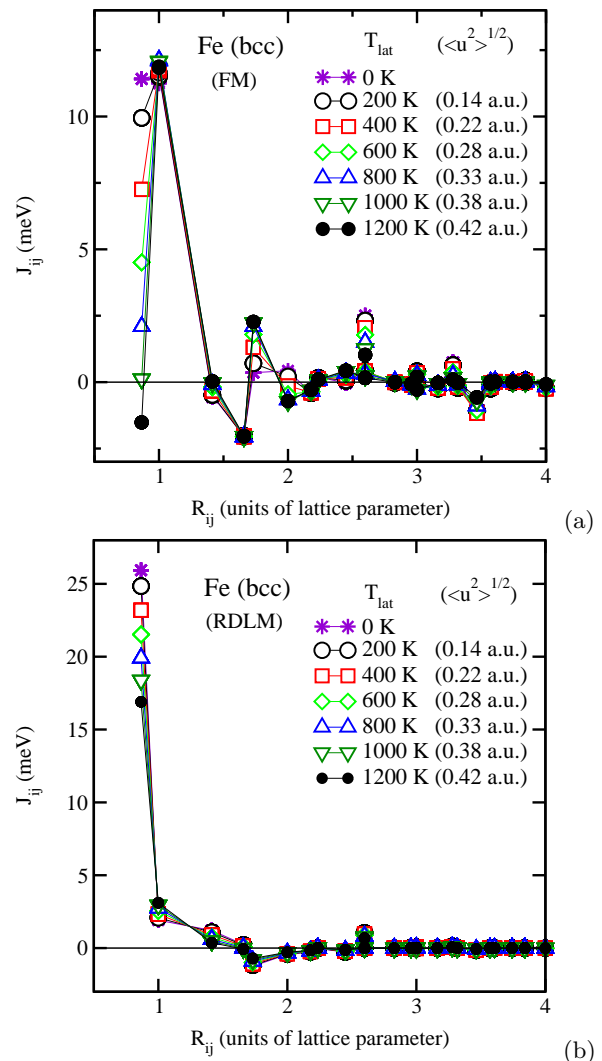


FIG. 1. The isotropic exchange coupling parameters J_{ij} for bcc Fe calculated for the FM (a) and DLM (b) reference states. The results are represented for different amplitudes of the thermal lattice vibrations given in terms of the rms displacement $(\langle u^2 \rangle_T)^{1/2}$ and corresponding *lattice temperature* T_{lat} .

obtained by summing J_{ij} within a sphere with radius $R_{\max} = 5a$, with a being the lattice parameter.

Fig. 2 (circles) shows corresponding results for T_C obtained via the MFA as a function of the temperature dependent rms displacements $(\langle u^2 \rangle_T)^{1/2}$. Keeping in mind that the mean field approximation (MFA) normally overestimates the critical temperature when compared to results obtained from Monte Carlo (MC) simulations or RPA (random phase approximation) based calculations, one notes that the MFA result for T_C of bcc Fe, evaluated without accounting for the lattice vibrations, is rather close to the experimental value, $T_C^{\text{exp}} = 1043$ K. However, a finite amplitude of the lattice vibrations leads to a significant monotoneous decrease of T_C^{MFA} with $(\langle u^2 \rangle_T)^{1/2}$ implying a corresponding deviation from experiment. As

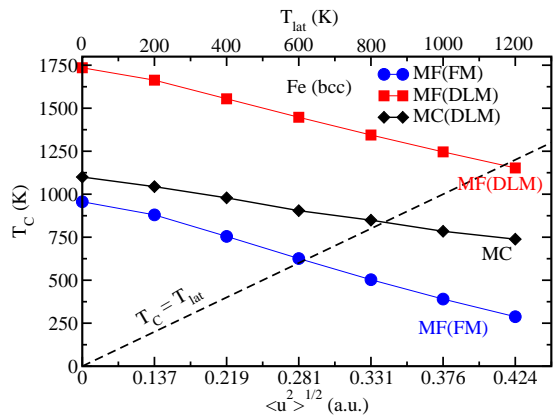


FIG. 2. Theoretical Curie temperature T_C plotted as a function of the amplitudes of thermal lattice vibrations $\langle (u^2)_T \rangle^{1/2}$ calculated for the FM and DLM reference states either using the MFA or MC simulations together with the relation between the *lattice temperature* T_{lat} and $\langle (u^2)_T \rangle^{1/2}$.

mentioned above, more reliable results for the Curie temperature can be obtained on the basis of the exchange coupling parameters calculated for the PM reference state described here within the disordered local moment (DLM) approximation. Using the non-relativistic version of this model, magnetic disorder in the PM state is accounted for by averaging over all possible directions of the spin moments. Equivalent to this, is to consider a pseudo alloy $Fe_{0.5}^{\text{up}}Fe_{0.5}^{\text{down}}$ of Fe atoms with opposite spin moments oriented up and down, respectively. Fig. 1 (b) gives the corresponding exchange coupling parameters of Fe for the PM reference state on the basis of the DLM Model. These parameters and their temperature dependence are quite different from those obtained for the FM reference state. As a consequence, the corresponding MFA Curie temperature (≈ 1700 K) exceeds the value obtained for the FM reference state in an appreciable way when thermal lattice vibrations are ignored. This observation was already reported in the literature before (see e.g. 26). A finite amplitude of the thermal atomic displacements leads again to a lower MFA-based Curie temperature, as it is shown in Fig. 2, reaching the value $T_C^{\text{MF}} \approx 1200$ K when requiring that the Curie temperature and *lattice temperature* coincide.

Fig. 2 (triangles) gives also results for the Curie temperature obtained by MC simulations considering 15 atomic shells around each atom using DLM-based exchange parameters. In this case, the Curie temperature T_C^{MC} , calculated for an unperturbed lattice slightly overestimates the experimental value. When the amplitude of thermal lattice vibrations increases, T_C^{MC} also goes down and coincides with the *lattice temperature* T_{lat} at around 1000 K underestimating slightly the experimental Curie temperature this way. This small deviation might among others be ascribed to the approximate treatment of lattice vibrations when calculating J_{ij} that in particular neglects correlations in the thermal motion of the atoms.

To get more insight concerning the temperature dependence of the exchange coupling parameters, Fig. 3 (a) shows the nearest neighbor parameter J_{01} for FM bcc Fe for two different temperatures as a function of the upper limit of the energy integration in Eq. (2) (with $E = 0$ eV the true Fermi energy) reflecting its dependence on the occupation. The solid and dashed lines

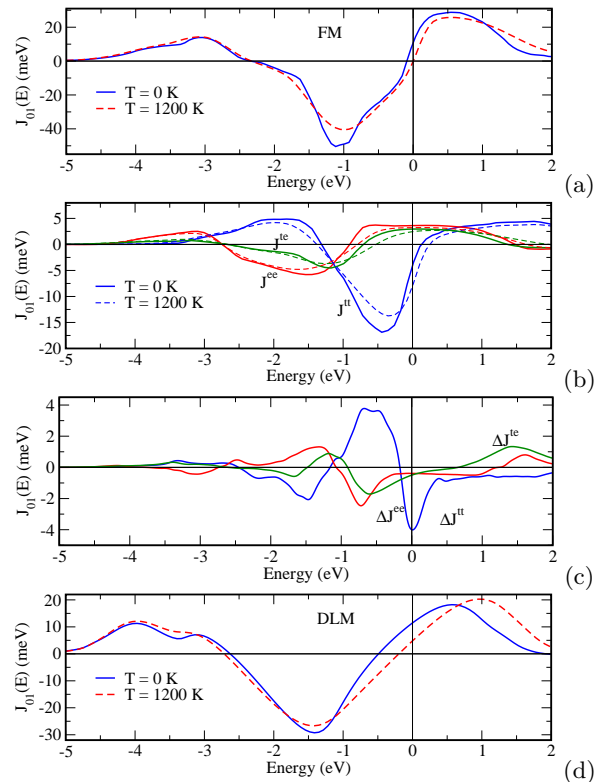


FIG. 3. The occupation dependence of the exchange coupling parameter J_{01} of bcc Fe for the FM (a) and the DLM (c) reference states. Dashed line represents results for the *lattice temperature* $T_{\text{lat}} = 1200$ K. (b) represents the orbital-resolved parameters for the FM reference state, \tilde{J}_{01}^{tt} , \tilde{J}_{01}^{ee} and \tilde{J}_{01}^{te} , respectively, while (c) gives their changes due to thermal lattice vibrations when increasing T_{lat} from 0 to 1200 K.

represent results obtained without and with lattice vibrations, respectively, accounted for. One can see, that depending on the occupation of the valence band the lattice vibrations can result either in a decrease or increase of the exchange parameter. Following Kvashnin *et al.*²⁷, one can further decompose J_{ij} into its orbital contributions. For the orbitals grouped according to the representations of the cubic point group, t_{2g} and e_g , the exchange parameter can be decomposed according to the expression $J_{ij} = J_{ij}^{t_{2g}-t_{2g}} + J_{ij}^{e_g-e_g} + J_{ij}^{t_{2g}-e_g}$ allowing to monitor the dependence of the individual orbital contributions to J_{ij} ¹⁷ on the lattice vibrations. In Fig. 3 (b) representative results are shown for the contributions of the $l = 2, m = \pm 1$ (t_{2g}) and $l = 2, m = 0$ orbitals (e_g) to the nearest neighbor interaction parameter J_{01} , with

the corresponding representations given in parentheses. To distinguish these data from those connected with the complete set of the cubic point group representations, t_{2g} and e_g , we use the symbol \tilde{J} instead of J . For calculations done without lattice vibrations ($T_{\text{lat}} = 0$ K), this decomposition reveals an antiferromagnetic character for the \tilde{J}_{01}^{tt} parameter in contrast to the ferromagnetic character of \tilde{J}_{01}^{ee} and \tilde{J}_{01}^{te} . This finding is in full agreement with previous work^{17,27}. The change of the orbital resolved coupling parameters $\tilde{J}_{01}^{\gamma\gamma'}$ ($\gamma(\gamma') = e \equiv e_g, t \equiv t_{2g}$) when going from 0 to 1200 K is shown in Fig. 3 (c). Obviously, the most pronounced changes are found for the contribution \tilde{J}_{01}^{tt} . The observed changes are primarily ascribed to the broadening of the electronic states due to the thermal lattice vibrations, leading either to an increase or decrease of $\tilde{J}_{01}^{\gamma\gamma'}$ or J_{01} , respectively, depending on the occupation of the energy band. Finally, Fig. 3 (d) represents results obtained for the DLM reference state. The electronic states in this case are broadened in addition due to the thermally induced magnetic disorder in the system. Including thermal lattice vibrations in addition with $T_{\text{lat}} = 1200$ K leads for the J_{01} parameter to changes w.r.t. $T_{\text{lat}} = 0$ K comparable to those found for the ferromagnetic reference state (see Fig. 3 (a))

The isotropic exchange coupling parameters J_{ij} calculated for fcc Ni are shown in Fig. 4. For this material the

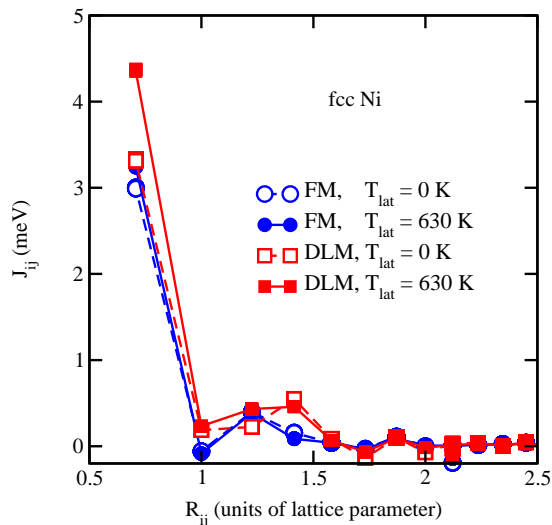


FIG. 4. Exchange coupling parameters J_{ij} calculated for Ni for the FM and DLM reference state without lattice vibrations and accounting for lattice vibrations corresponding to $T_{\text{lat}} = 630$ K.

lattice vibrations lead to a tiny modification of the exchange parameters calculated for the FM reference state as the results for $T_{\text{lat}} = 0$ (circles) and 630 K (triangles) shown in Fig. 4 demonstrate. The mean-field Curie temperature evaluated with these parameters increases from $T_C^{\text{MF}} \approx 420$ K obtained with the parameters for the unperturbed ground state ($T_{\text{lat}} = 0$ K) to $T_C^{\text{MF}} \approx 430$ K

for the state with an amplitude of lattice vibrations corresponding to $T_{\text{lat}} = 630$ K. The well known itinerant-electron character of magnetism in Ni leads – in contrast to Fe – for the PM state above the Curie temperature to a very small or vanishing magnetic moment (see e.g. Ref. 28 and references therein). This prevents to perform standard self-consistent DLM calculations as these also lead to a zero local magnetic moment for the paramagnetic DLM state. For that reason, Ruban *et al.* suggested to use a constrained local exchange field when dealing with the magnetic properties of Ni. As the subtle temperature dependent magnetism of Ni is not the central issue of the present work, we investigated the simultaneous impact of lattice vibrations and magnetic disorder on the J_{ij} parameters by performing the DLM-like calculations with the spin moment constrained by using a frozen potential^{1,4,5}. The resulting exchange coupling parameters calculated for the DLM reference state without account for lattice vibrations are given in Fig. 4 by open squares, while closed squares represent data for the *lattice temperature* $T_{\text{lat}} = 630$ K. As one notes, the first-neighbor exchange parameters significantly increase with the temperature increase as can be seen in Fig. 4. The corresponding MFA Curie temperature shown in Fig. 5 by squares increases from ~ 470 K for $T_{\text{lat}} = 0$ K to ~ 600 K for $T_{\text{lat}} = 630$ K. However, one should keep in

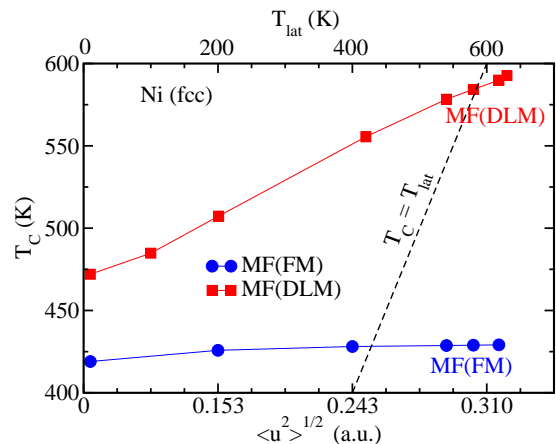


FIG. 5. The MF Curie temperature calculated for fcc Ni for the FM and DLM reference states, plotted as a function of the amplitudes of thermal lattice vibrations given in terms of *lattice temperature*.

mind that the MFA results lead usually to an overestimation of the Curie temperature. On the other hand, performing instead MC simulations based on the DLM derived exchange parameters calculated for $T_{\text{lat}} = 630$ K, leads to a Curie temperature $T_C = 430$ K that is far below the experimental value.

The occupation dependence of the exchange coupling parameter J_{01} of Ni calculated for the FM reference state is shown in Fig. 6 (a) for the two *lattice temperatures* $T_{\text{lat}} = 0$ and 630 K. As to be expected from Fig. 4 a relatively weak impact of thermal lattice vibrations is found

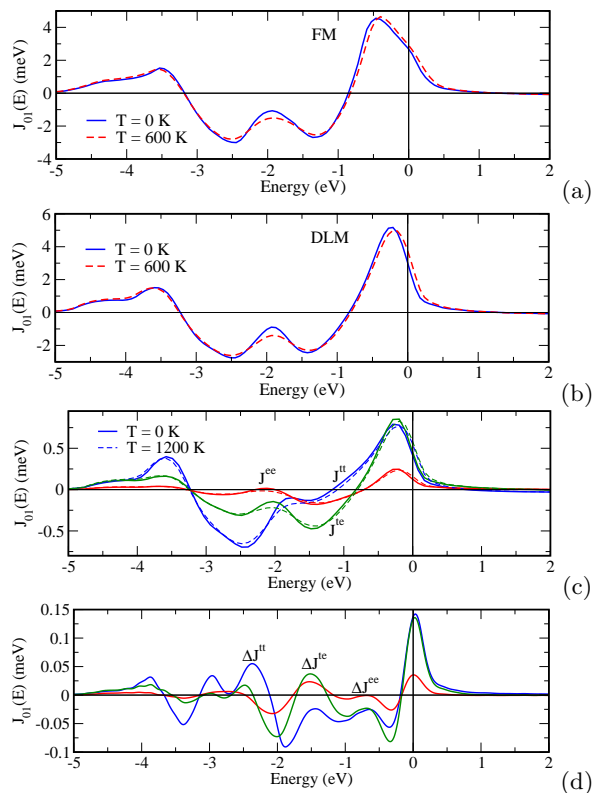


FIG. 6. The occupation dependent exchange coupling parameter J_{01} for fcc Ni for the FM (a) and the DLM (b) reference states. (c) represents the orbital decomposed parameters for the DLM reference state, \tilde{J}_{01}^{tt} , \tilde{J}_{01}^{ee} and \tilde{J}_{01}^{te} and (d) their changes due to thermal lattice vibrations.

in this case. This can partially be attributed to the rather low critical temperature, i.e. temperature regime to be considered, for which the mean-square displacements of the atoms are still too small to lead to significant changes in the electronic structure. In line with this, the temperature dependence of the parameter for the DLM reference state shown in Fig. 6 (b) is found to be very similar to that for the FM state. The orbital decomposition of the data for the DLM reference state that is given in Fig. 6 (c) shows that all components \tilde{J}_{01}^{tt} , \tilde{J}_{01}^{ee} and \tilde{J}_{01}^{te} are positive for the occupation corresponding to the true Fermi energy of fcc Ni and that for Ni the most pronounced impact of lattice vibrations occurs for the \tilde{J}_{01}^{tt} and \tilde{J}_{01}^{te} contributions.

As an example for a compound, the well known B2 FeRh system that exhibits a temperature induced AFM to FM transition is considered in the following. According to first-principles calculations²⁹, the metamagnetic transition can be seen as a result of the competition of Fe-Fe exchange interactions including indirect Fe-Rh-Fe interactions, which depend on the magnetic configuration. However, a possible influence of lattice vibrations on the finite temperature magnetic properties of FeRh has not been discussed so far. Within the present work, calculations have been performed for the FM and

AFM configurations separately considering several values of *lattice temperatures*. The corresponding results are given in Fig. 7 for the FM (a) and AFM (b) states. One can see in both cases that the increase of the am-

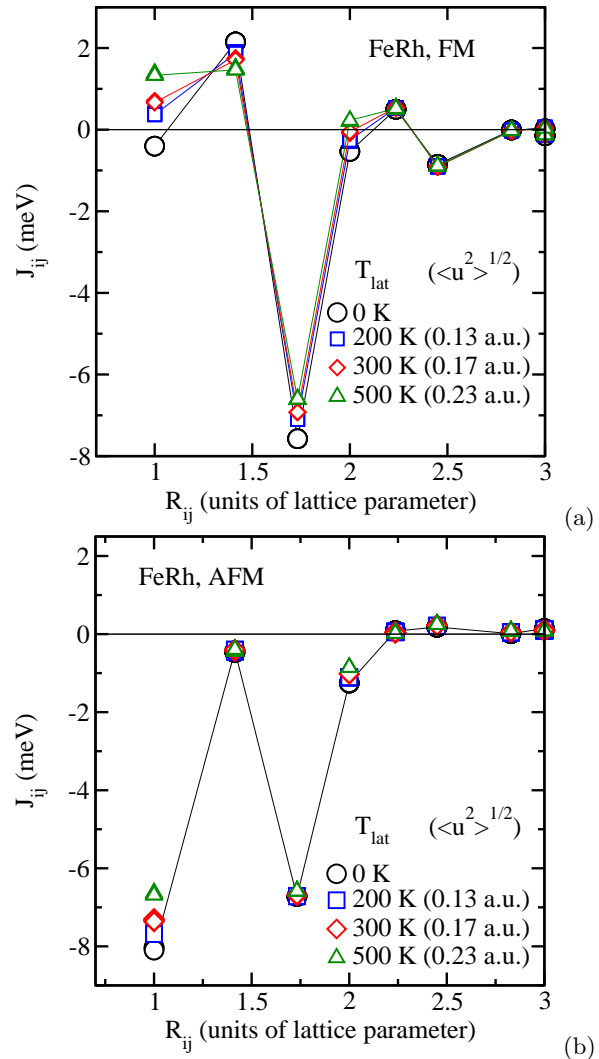


FIG. 7. Interatomic Fe-Fe exchange coupling parameters corresponding to various temperatures, calculated for FeRh with the FM (a) and AFM (b) structures. The temperature dependency is only due to the thermal lattice vibrations. The mean-square displacements corresponding to the considered temperatures are as follows: 0.13 a.u. (200 K), 0.17 a.u. (300 K), and 0.23 a.u. (500 K).

plitude of the thermal lattice vibrations results in an increase of the interatomic FM exchange and a decrease of the AFM exchange interactions. This implies that thermal lattice vibrations should decrease the stability of the low-temperature AFM phase upon heating via the induced changes of the exchange parameters for the FM as well as AFM state. This should result in a decrease by about 40 K (using the *lattice temperature* $T_{lat} = 300$ K) of the critical temperature of the AFM-FM metamagnetic phase transition, that follows from the MC simulations.

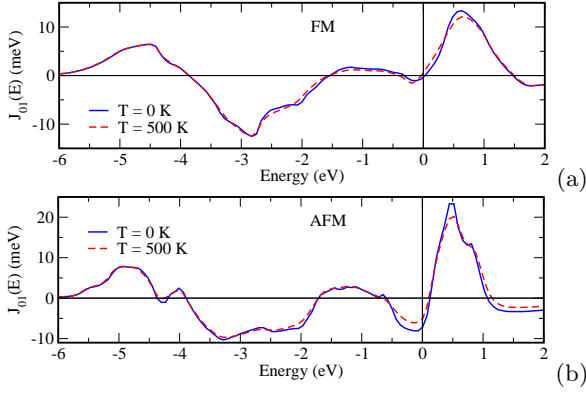


FIG. 8. The occupation dependent Fe-Fe exchange coupling parameter J_{01} for FeRh using the FM (a) and the AFM (b) structure as a reference states. The results are presented for two values of the *lattice temperature* T_{lat} .

Note however, that these calculations do not account for the impact of lattice vibrations on the Fe-Rh exchange interactions.

The occupation dependence of the Fe-Fe exchange coupling parameter J_{01} of FeRh are shown in Fig. 8 for the FM as well as the AFM reference states. One can see that the impact of lattice vibrations on J_{ij} is rather small over all occupation numbers or energies, respectively, and is close to its maximum value for the proper occupation number at the Fermi level, i.e. at $E = 0$ eV.

Finally, as an example for two-dimensional systems, we present results for 1ML Fe on a Pt (111) and Au (111) substrate, respectively. The lack of inversion symmetry leads to non-vanishing Dzyaloshinskii-Moriya interactions (DMI) in these systems. Therefore we will discuss here the impact of lattice vibrations not only on the isotropic exchange but also on the anisotropic interactions. As the Curie temperatures evaluated within the MFA are ≈ 800 K for Fe/Pt(111) and ≈ 900 K for Fe/Au(111), the highest *lattice temperature* used in our calculations is 900 K. Figs. 9 and 10 show results for the Fe-Fe isotropic exchange interaction (a), the x - (b) and the z -component (c) of the DMI, calculated for the FM reference state of these systems. As one can see, in both cases a similar behavior has been found for isotropic exchange interactions J_{ij} as a function of the Fe-Fe distance R_{ij} with a weak dependency on the lattice temperature. On the other hand, the dependence of the DMI components, D_{ij}^{α} , on thermal lattice vibrations is much more pronounced. Interestingly, an opposite trend of the temperature induced modifications of the D_{ij}^{α} parameters shows up for different Fe-Fe distances. A similar behavior can also be seen when comparing the first-neighbor DMI for the systems under consideration. While in the case of 1ML Fe/Au(111) an increasing amplitude of thermal lattice vibrations results in a decrease of the Fe-Fe DMI (see Fig. 10 (b)), the DMI increases with increasing *lattice temperature* in the case of 1ML Fe/Pt(111). To get more insight concerning the influence of lattice vibra-

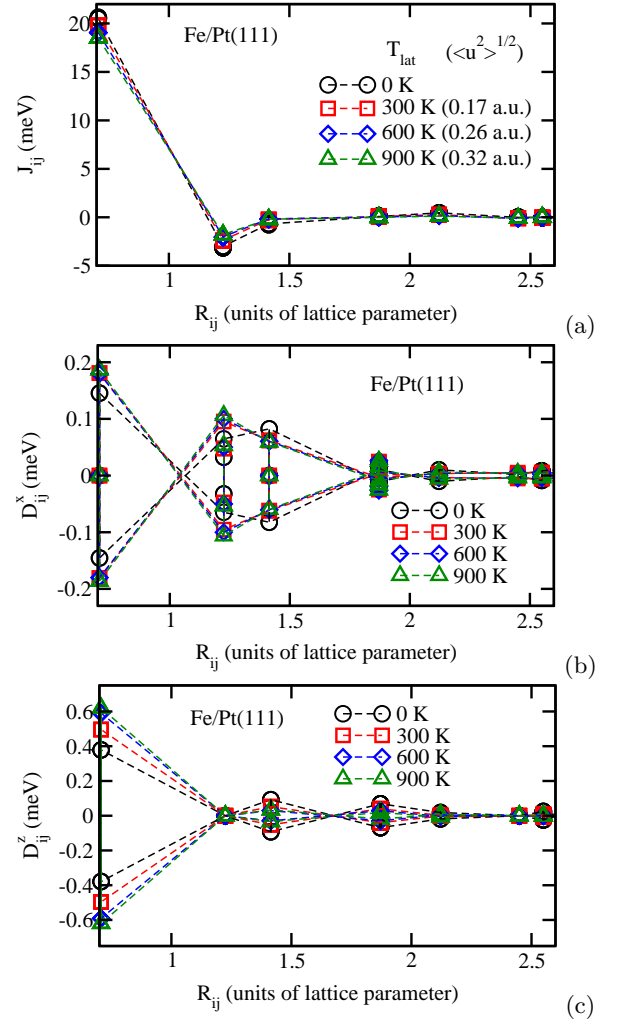


FIG. 9. The isotropic exchange coupling parameter J_{ij} (a), the x -component D_{ij}^x (b) and the z -component D_{ij}^z (c) of the DMI for 1ML Fe on the Pt(111) surface for several values of the rms atomic displacement $(\langle u^2 \rangle_T)^{1/2}$ (given in parentheses) corresponding to different *lattice temperatures* T_{lat} .

tions on the exchange interactions, the nearest-neighbor exchange parameters have been calculated as a function of occupation for two different values of the lattice temperature. Figs. 12 and 13 show the isotropic Fe-Fe exchange coupling parameter J_{01} (a) and z -component of the DMI, D_{01}^z (b). For the parameter J_{01} only a weak change caused by an increase of the *lattice temperature* can be seen over whole regime of occupation numbers represented in the figures. In contrast to this, Figs. 12 (b) and 13 show a very pronounced impact of the lattice vibrations on the parameter D_{01}^z . As one can see in the figures, D_{01}^z seen as a function of the occupation, has a non-monotonous behavior at low temperature with the observed 'fine structure' associated with avoided crossings of the energy bands. These details of the electronic structure can be seen in Fig. 11 (a) for 1ML Fe/Pt(111) in the vicinity of the Fermi energy. The rapid changes of

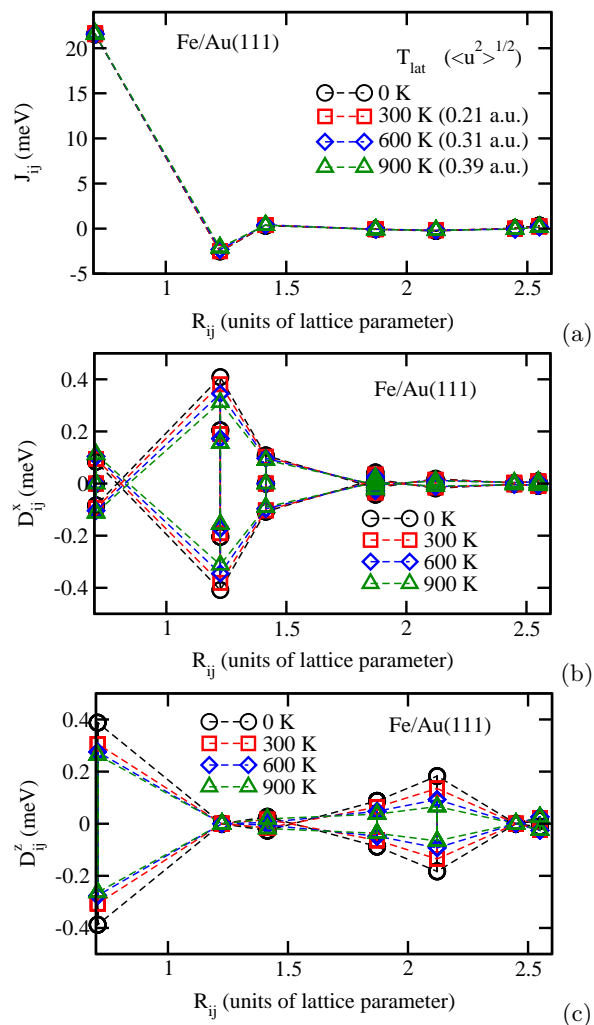


FIG. 10. The isotropic exchange coupling parameter J_{ij} (a), the x-component D_{ij}^x (b) and the z-component D_{ij}^z (c) of the DMI for 1ML Fe/Au(111) for several values of the rms atomic displacement $(\langle u^2 \rangle_T)^{1/2}$ (given in the parentheses) corresponding to different lattice temperatures T_{lat} .

the DMI occur when the apparently varied Fermi level passes through an avoided crossing of the energy bands (see discussion in^{30,31}). The prominent features in the DMI plots seen in Figs. 12 (b) and 13 (b) are created by those energy bands that give a dominant contribution to D_{01}^z . When the lattice temperature increases to $T_{lat} = 900$ K, the 'fine structure' of $D_{01}^z(E)$ seen as a function of E is washed out for both systems. Partially, this can be attributed to a smearing of the energy bands due to an increasing electron scattering by the thermal lattice vibrations. This mechanism is demonstrated in Fig. 11 (b) that represents the Bloch spectral function calculated for an imaginary part of the energy of 5 meV mimicking a decrease of the life time of the electronic states connected with the electron scattering by lattice vibrations. This modification of the electronic structure leads for 1ML Fe/Pt(111) to the changes of $J_{01}(E)$ and

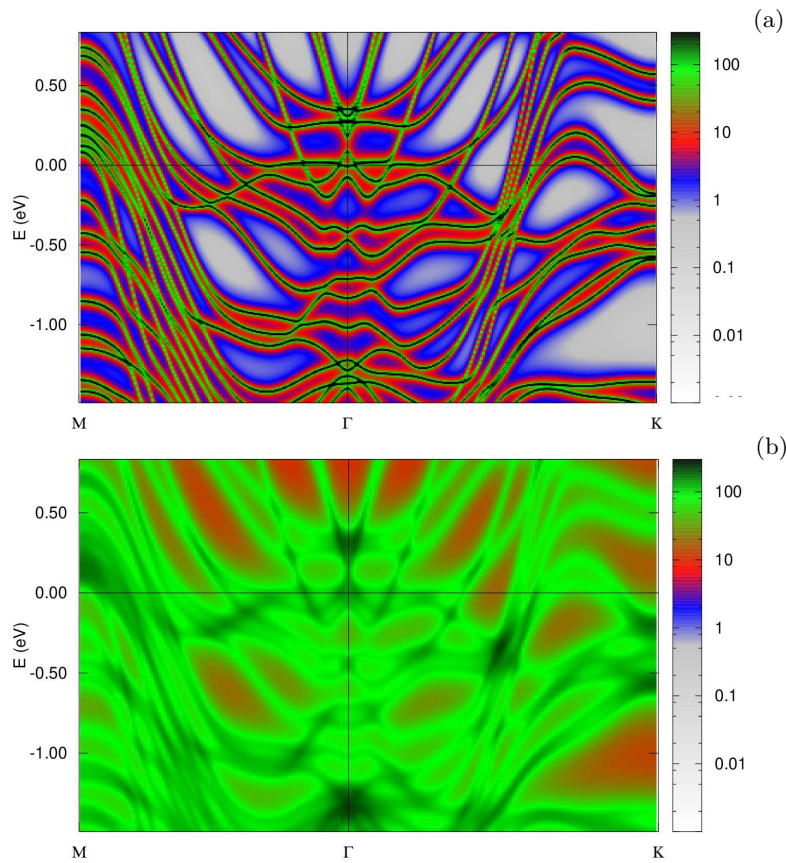


FIG. 11. The Bloch spectral function calculated for 1ML Fe/Pt(111) using two values of the imaginary part of the energy: 0.1 meV (a) and 5 meV (b).

$D_{01}^z(E)$ as function of the energy shown in Fig. 12 (a) and (b) by dotted lines. Dashed-dotted lines represent corresponding results obtained for an imaginary part of the energy of 10 meV. In the case of the DMI, one can see a decrease of the amplitude of modulations with energy when the imaginary part of the energy increases. However, comparing these results with the results obtained for $T_{lat} = 900$ K, it is obvious that the influence of thermal lattice vibrations on the exchange parameters also stems to a large extent from their impact on the matrix elements given in Eq. (3).

IV. SUMMARY

To summarize, the alloy analogy model was used to calculate the exchange coupling parameters taking into account randomly distributed atomic displacements in the lattice giving access this way to temperature induced modifications of the exchange parameters. Focusing both on the isotropic exchange and Dzyaloshinskii-Moriya interactions, it is demonstrated that – depending on the material – the effect of lattice vibrations on the exchange parameters can be rather significant and should be taken into account in simulations of finite-temperature mag-

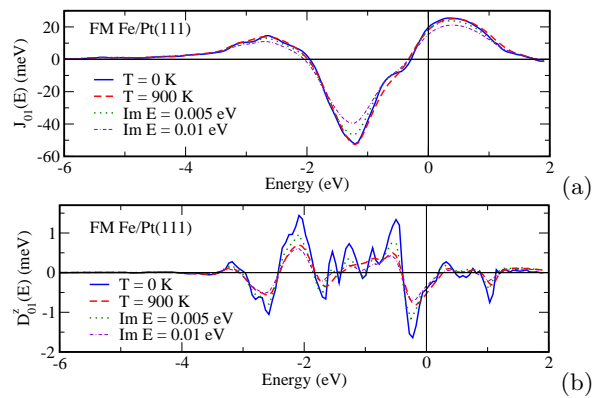


FIG. 12. The occupation dependent Fe-Fe exchange coupling parameter J_{01} (a) and z-component of the DMI D_{01}^z in 1ML Fe/Pt(111) calculated for two values of the *lattice temperature* T_{lat} . Dotted and dashed-dotted lines represent the results obtained with the imaginary energy part of 5 and 10 meV, respectively.

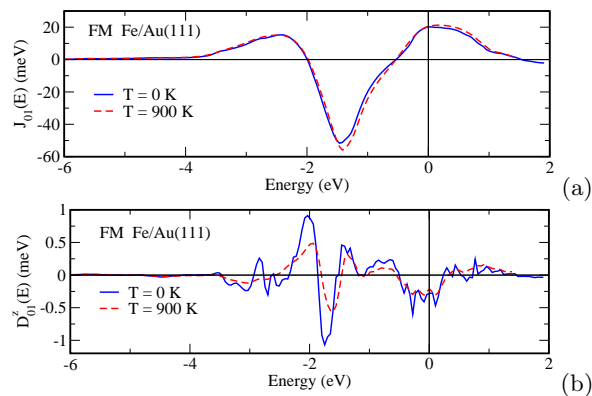


FIG. 13. The occupation dependent Fe-Fe exchange coupling parameter J_{01} (a) and z-component of the DMI D_{01}^z in 1ML Fe/Au(111) calculated for two values of the *lattice temperature* T_{lat} .

netic properties of these systems. Moreover, the present approach allows to make a corrections to the exchange coupling parameters in random alloys with alloy components having different atomic radius resulting in turn in randomly distributed atomic displacements, e.g. in high-entropy alloys characterized by rather significant static mean-square atomic displacements³².

V. ACKNOWLEDGMENT

Financial support by the DFG via SFB 1277 (Emergent Relativistic Effects in Condensed Matter - From Fundamental Aspects to Electronic Functionality) is gratefully acknowledged.

-
- ¹ H. Ebert, S. Mankovsky, K. Chadova, S. Polesya, J. Minár, and D. Ködderitzsch, Phys. Rev. B **91**, 165132 (2015).
 - ² W. H. Butler, Phys. Rev. B **31**, 3260 (1985).
 - ³ B. Velický, Phys. Rev. **184**, 614 (1969).
 - ⁴ H. Ebert, S. Mankovsky, D. Ködderitzsch, and P. J. Kelly, Phys. Rev. Lett. **107**, 066603 (2011), <http://arxiv.org/abs/1102.4551v1>.
 - ⁵ S. Mankovsky, D. Ködderitzsch, G. Woltersdorf, and H. Ebert, Phys. Rev. B **87**, 014430 (2013).
 - ⁶ B. L. Gyorffy, A. J. Pindor, J. Staunton, G. M. Stocks, and H. Winter, J. Phys. F: Met. Phys. **15**, 1337 (1985).
 - ⁷ B. L. Gyorffy, A. Barbieri, J. B. Staunton, W. A. Shelton, and G. M. Stocks, Physica B **172**, 35 (1991).
 - ⁸ J. B. Staunton and B. L. Gyorffy, Phys. Rev. Lett. **69**, 371 (1992).
 - ⁹ J. B. Staunton, L. Szunyogh, A. Buruzs, B. L. Gyorffy, S. Ostanin, and L. Udvardi, Phys. Rev. B **74**, 144411 (2006).
 - ¹⁰ A. Buruzs, P. Weinberger, L. Szunyogh, L. Udvardi, P. I. Chleboun, A. M. Fischer, and J. B. Staunton, Phys. Rev. B **76**, 064417 (2007).
 - ¹¹ D. Böttcher, A. Ernst, and J. Henk, Journal of Magnetism and Magnetic Materials **324**, 610 (2012).
 - ¹² L. Szunyogh and L. Udvardi, Phil. Mag. **78**, 617 (1998).
 - ¹³ R. F. Sabiryanov and S. S. Jaswal, Phys. Rev. Lett. **83**, 2062 (1999).
 - ¹⁴ S. Mankovsky, S. Polesya, H. Ebert, W. Bensch, O. Mathon, S. Pascarelli, and J. Minár, Phys. Rev. B **88**, 184108 (2013).
 - ¹⁵ B. Alling, F. Körmann, B. Grabowski, A. Glensk, I. A. Abrikosov, and J. Neugebauer, Phys. Rev. B **93**, 224411 (2016).
 - ¹⁶ E. Mozafari, B. Alling, M. P. Belov, and I. A. Abrikosov, Phys. Rev. B **97**, 035152 (2018).
 - ¹⁷ A. V. Ruban and O. E. Peil, Phys. Rev. B **97**, 174426 (2018).

- ¹⁸ M. Di Gennaro, A. L. Miranda, T. A. Ostler, A. H. Romero, and M. J. Verstraete, *Phys. Rev. B* **97**, 214417 (2018).
- ¹⁹ L. Udvardi, L. Szunyogh, K. Palotás, and P. Weinberger, *Phys. Rev. B* **68**, 104436 (2003).
- ²⁰ H. Ebert and S. Mankovsky, *Phys. Rev. B* **79**, 045209 (2009).
- ²¹ M. E. Rose, *Relativistic Electron Theory* (Wiley, New York, 1961).
- ²² H. Ebert, J. Braun, D. Ködderitzsch, and S. Mankovsky, *Phys. Rev. B* **93**, 075145 (2016).
- ²³ H. Ebert, D. Ködderitzsch, and J. Minár, *Rep. Prog. Phys.* **74**, 096501 (2011).
- ²⁴ H. Ebert et al., *The Munich SPR-KKR package*, version 7.7, <https://www.ebert.cup.uni-muenchen.de/en/software-en/13-sprkk> (2017).
- ²⁵ S. H. Vosko, L. Wilk, and M. Nusair, *Can. J. Phys.* **58**, 1200 (1980), <http://www.nrcresearchpress.com/doi/pdf/10.1139/p80-159>.
- ²⁶ A. Buruzs, L. Szunyogh, and P. Weinberger, *Phil. Mag.* **88**, 2615 (2008).
- ²⁷ Y. O. Kvashnin, R. Cardias, A. Szilva, I. Di Marco, M. I. Katsnelson, A. I. Lichtenstein, L. Nordström, A. B. Klautau, and O. Eriksson, *Phys. Rev. Lett.* **116**, 217202 (2016).
- ²⁸ A. V. Ruban, S. Khmelevskiy, P. Mohn, and B. Johansson, *Phys. Rev. B* **75**, 054402 (2007).
- ²⁹ S. Polesya, S. Mankovsky, D. Ködderitzsch, J. Minár, and H. Ebert, *Phys. Rev. B* **93**, 024423 (2016).
- ³⁰ T. Koretsune, N. Nagaosa, and R. Arita, *Scientific Reports* **5**, 13302 (2015).
- ³¹ L. M. Sandratskii, *Phys. Rev. B* **96**, 024450 (2017).
- ³² S. Mu, G. D. Samolyuk, S. Wimmer, M. C. Troparevsky, S. N. Khan, S. Mankovsky, H. Ebert, and G. M. Stocks, *npj Computational Materials* **5**, 1 (2019).